SUPPLEMENTARY MATERIAL

METHODS

Proteins and buffers. Brain tubulin was purified by two cycles of polymerization in a high molarity buffer (0.33 M PIPES-K pH 6.9, 33% glycerol, 3.3 mM $MgCl_2$, 6.7 mM EGTA, 0.5 mM GTP, 1.5 mM ATP) (Castoldi and Popov, 2003) and depolymerization (in 50 mM Mes-K pH 6.6, 1 mM $CaCl_2$, 1 mM 2-Mercaptoethanol) and finally stored at –80°C in 50 mM Mes-K pH 6.8, 33% glycerol, 0.25 mM $MgCl_2$, 0.5 mM EGTA, 0.1 mM GTP until use. Before each experiment, an additional MT assembly was performed, followed by disassembly in P buffer (80 mM PIPES-K, pH 6.8, 1 mM $MgCl_2$, 0.5 mM EGTA) containing 2 mM GDP; buffer was subsequently exchanged on a 8.3 ml bed volume Sephadex G-25 column (PD-10, Amersham) equilibrated in a buffer that is described for each experiment. Tubulin concentrations were deduced from its absorbance (e_{278}= 1.23 ml cm^{-1} mg^{-1}), assuming the molecular weight of the heterodimer is 100 kDa (Correia et al., 1987). To prepare tubulin-colchicine, colchicine (Fluka) in excess (1 mM) was included in the depolymerization step in P buffer and the unbound drug was removed on the following buffer exchange column. The colchicine concentration was estimated from its absorbance at 351 nm (e_{351}=16218). Two sources of tubulin were used, sheep or bovine brain. All structures were determined with bovine brain tubulin and most biochemical experiments were with ovine brain tubulin. We checked that the GTPase inhibition results are identical irrespective of the brain tubulin source used and that the results of tubulin nucleotide exchange assays are identical to those reported by others who used a bovine brain source (Bai et al., 1990).

The RB3 Stathmin like domain (RB3-SLD) was expressed and purified as previously described (Charbaut et al., 2001) and the C-terminal helix of RB3 (Rhel, residues 46 - 138, stathmin numbering) was purified as described for similar fragments of stathmin (Redeker et al., 2000). The SLD concentration was determined by amino acid analysis or by titrating a

known tubulin solution with the SLD on a gel filtration column (Superose 12 10/300, Amersham). Both methods gave similar results.

Structure determination. Diffraction data were processed with the HKL suite (Otwinowsky and Minor, 1997). The $(Tc)_2R$ structure was used as a starting model and further refined as in (Gigant et al., 2005) with REFMAC (CCP4, 1994), using the TLS option (Winn et al., 2001). The strongest features of the extra density in a Fobs-Fcalc omit map were attributed to the soaked compounds, thus identifying one (soblidotin and tripeptide) or two (phomopsin A) such molecules per $(Tc)_2R$. The X-ray structure of phomopsin A (Culvenor et al., 1989) was used as a starting model in refinement, whereas for soblidotin we used a truncated energy minimized model of dolastatin 10 (Mitra and Sept, 2004). Topology parameters were generated using the program PRODRG (Schuttelkopf and van Aalten, 2004). Statistics for data processing and refinement are summarised in the Supplementary Table. We used the O program for structure visualisation and manual rebuilding (Jones et al., 1991).

Figures were generated with MOLSCRIPT (Kraulis, 1991), BOBSCRIPT (Esnouf, 1997), RASTER 3D (Meritt and Bacon, 1997) and PYMOL (DeLano, 2002).

GTPase activity measurements. Varying concentrations of ligands were added to a 5 µM $(Tc)_2R$ solution in P-buffer for a 20 min incubation at 4°C. Measurements of the GTPase activity were started after adding 150 µM [γ-^{32}P] GTP and prewarming the samples for 6 min at 37°C. As dolastatin 10 and phomopsin A inhibit tubulin nucleotide exchange (Hamel, 1992 and our unpublished observations), we checked that similar results are obtained when tubulin is loaded with GTP before addition of RB3-SLD and of the vinca domain ligand. This demonstrates that soblidotin and phomopsin A inhibit GTP hydrolysis by $(Tc)_2R$, in addition to nucleotide exchange. Free inorganic phosphate was quantified during a 24 minutes time course by extracting it as a phosphomolybdate complex as described (Wang et al., 2007). The slope of the plot of the concentration of inorganic phosphate as a function of time gives the total GTPase activity of each sample; the average specific activity of tubulin was derived by

dividing the background-subtracted total activity by the tubulin concentration. The $(Tc)_2R$-ligand affinity constant was extracted from the analysis of the inhibition of the GTPase activity as a function of ligand concentration, as in (Wang et al., 2007). The GTPase activity of tubulin-colchicine was measured in a modified P buffer containing 250 mM PIPES-K.

REFERENCES

Bai, R.L., Pettit, G.R. and Hamel, E. (1990) Binding of dolastatin 10 to tubulin at a distinct site for peptide antimitotic agents near the exchangeable nucleotide and vinca alkaloid sites. *J Biol Chem*, **265**, 17141-17149.

Castoldi, M. and Popov, A.V. (2003) Purification of brain tubulin through two cycles of polymerization-depolymerization in a high-molarity buffer. *Protein Expr Purif*, **32**, 83-88.

CCP4. (1994) The CCP4 suite: programs for protein crystallography. *Acta Crystallogr D*, **50**, 760-763.

Charbaut, E., Curmi, P.A., Ozon, S., Lachkar, S., Redeker, V. and Sobel, A. (2001) Stathmin family proteins display specific molecular and tubulin binding properties. *J Biol Chem*, **276**, 16146-16154.

Correia, J.J., Baty, L.T. and Williams, R.C., Jr. (1987) Mg2+ dependence of guanine nucleotide binding to tubulin. *J Biol Chem*, **262**, 17278-17284.

Culvenor, C.C.J., Edgar, J.A., MacKay, M.F., Gorst-Allman, C.P., Marasas, W.F.O., Steyn, P.S., Vleggaar, R. and Wessels, P.L. (1989) Structure elucidation and absolute configuration of phomopsin a, a hexapeptide mycotoxin produced by phomopsis leptostromiformis. *Tetrahedron*, **45**, 2351-2372.

DeLano, W.L. (2002) The PyMOL Molecular Graphics System. DeLano Scientific.

Esnouf, R.M. (1997) An extensively modified version of MolScript that includes greatly enhanced coloring capabilities. *J Mol Graph*, **15**, 133-138.

Gigant, B., Wang, C., Ravelli, R.B., Roussi, F., Steinmetz, M.O., Curmi, P.A., Sobel, A. and Knossow, M. (2005) Structural basis for the regulation of tubulin by vinblastine. *Nature*, **435**, 519-522.

Hamel, E. (1992) Natural products which interact with tubulin in the vinca domain: maytansine, rhizoxin, phomopsin A, dolastatins 10 and 15 and halichondrin B. *Pharmacol Ther*, **55**, 31-51.

Jones, T.A., Zhou, J.-Y., Cowan, S.W. and Kjeldgaard, M. (1991) Improved methods for building protein models in electron density maps and the location of errors in these models. *Acta Crystallogr A*, **47**, 110-119.

Kraulis, P. (1991) MOLSCRIPT: a program to produce both detailed and schematic plots of proteins structures. *J Appl Crystallogr*, **24**, 946-950.

Meritt, E.A. and Bacon, D.J. (1997) Raster3D: Photorealistic Molecular Graphics. In Carter, C.W. and Sweet, R.M. (eds.), *Macromolecular Crystallography - Part B*. Academic Press, New York, Vol. 276, pp. 505-524.

Mitra, A. and Sept, D. (2004) Localization of the antimitotic peptide and depsipeptide binding site on beta-tubulin. *Biochemistry*, **43**, 13955-13962.

Otwinowsky, Z. and Minor, W. (1997) Processing of X-Ray Diffraction Data Collected in Oscillation Mode. In Carter, C.W.J. and Sweet, R.M. (eds.), *Methods in Enzymology*. Academic Press, New York, Vol. 276, pp. 307-325.

Redeker, V., Lachkar, S., Siavoshian, S., Charbaut, E., Rossier, J., Sobel, A. and Curmi, P.A. (2000) Probing the native structure of stathmin and its interaction domains with tubulin. *J Biol Chem*, **275**, 6841-6849.

Schuttelkopf, A.W. and van Aalten, D.M. (2004) PRODRG: a tool for high-throughput crystallography of protein-ligand complexes. *Acta Crystallogr D*, **60**, 1355-1363.

Wang, C., Cormier, A., Gigant, B. and Knossow, M. (2007) Insight into the GTPase activity of tubulin from complexes with stathmin-like domains. *Biochemistry*, **46**, 10595-10602.

Winn, M.D., Isupov, M.N. and Murshudov, G.N. (2001) Use of TLS parameters to model anisotropic displacements in macromolecular refinement. *Acta Crystallogr D*, **57**, 122-133.

Supplementary Table Data collection and refinement statistics

	$(Tc)_2R$ – phomopsin A	$(Tc)_2R$ – soblidotin
Data collection		
Space group	$P6_5$	$P6_5$
Cell dimensions		
a, *c* (Å)	327.1, 53.7	324.6, 53.3
Resolution (Å)	40 - 4.1 (4.2-4.1)*	35 –3.8 (3.87-3.8)*
R_{sym}	0.078 (0.428)	0.063 (0.469)
$I / \sigma I$	12.2 (1.9)	20 (2.3)
Completeness (%)	96 (90.8)	98.3 (94.9)
Redundancy	2.6 (2.6)	4.6 (3.5)
Refinement		
Resolution (Å)	20 – 4.1	20.0 – 3.8
No. reflections	25389	31414
R_{work} / R_{free}	0.215 / 0.265	0.229 / 0.295
No. atoms		
Protein	13981	14116
Ligand/ion	292	230
B-factors		
Protein	96 **	95 **
Ligand/ion	96 **	95 **
R.m.s. deviations		
Bond lengths (Å)	0.017	0.016
Bond angles (°)	2.04	1.96

*The dataset were collected from a single crystal in both cases. Values in parentheses are for the highest-resolution shell.

**Average of the individual temperature factors, to which the contribution of TLS as calculated by REFMAC should be added.

LEGENDS TO SUPPLEMENTARY FIGURES

Supplementary Figure 1: The β2 site of phomopsin A in $(Tc)_2R$. The β2-tubulin bound phomopsin A and its σ_a-weighted Fobs-Fcalc omit map contoured at 3.5 σ are presented.

Supplementary Figure 2: Structure-activity relationships of the 13-member ring of phomopsin A and ustiloxins. Phomopsin A in its high affinity binding site in $(Tc)_2R$ is in cyan, with C5 and C12 substituents highlighted. C10, which bears a linear appendage in ustiloxins A and B is presented as a black sphere. Vinblastine, positioned as in figure 2b, is in magenta (catharanthine) and lighter magenta (vindoline).

Supplementary Figure 3: Electron micrographs of negatively stained assemblies made of (a) $(Tc)_2$Rhel-vinblastine (as in Gigant et al., 2005), (b) $(Tc)_2$Rhel-phomopsin A and (c) $(Tc)_2$Rhel-soblidotin. Scale bar: 100 nm.

Supplementary Figure 4: Inhibition of tubulin GTPase activity. The variation of the specific GTPase activity of tubulin-colchicine is presented as a function of the concentration of phomopsin A (•) and soblidotin (o).

Supplementary Figure 5: The high affinity phomopsin A binding site and the interference between phomopsin A and the assembly of tubulin in straight protofilaments. The high affinity binding site for phomopsin A in $(Tc)_2R$ is depicted (color coded as in Fig. 1b). An α subunit in the conformation it adopts in MTs (grey) is also positioned relative to a phomopsin A-bound β subunit as across an inter dimer MT longitudinal interface. In addition to steric clashes with the two β tubulin loops of the vinca domain, the α subunit is prevented from occupying this position due to extensive overlap of phomopsin A with helix H10 and strands S8 and S9, as already seen with vinblastine, and with loop T7 (these elements highlighted in orange). The same interferences would occur with soblidotin (not shown).

Supplementary Figure 6: Stereoscopic view of the vinca domain in $(Tc)_2R$, with bound soblidotin. A σ_a-weighted Fobs-Fcalc omit map contoured at 4. σis represented. Color codes as in Figure 1c.

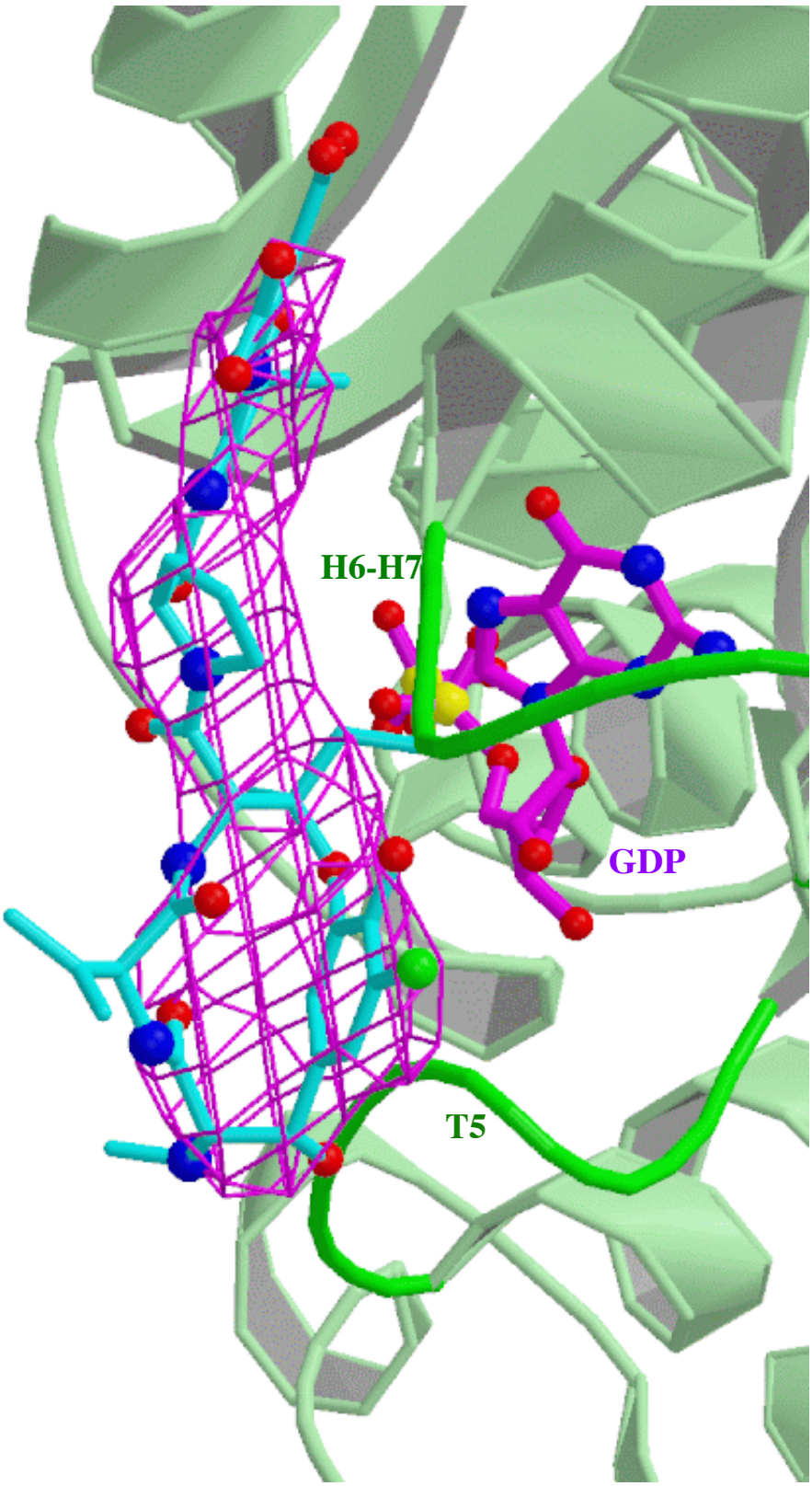

Supplementary Figure 1

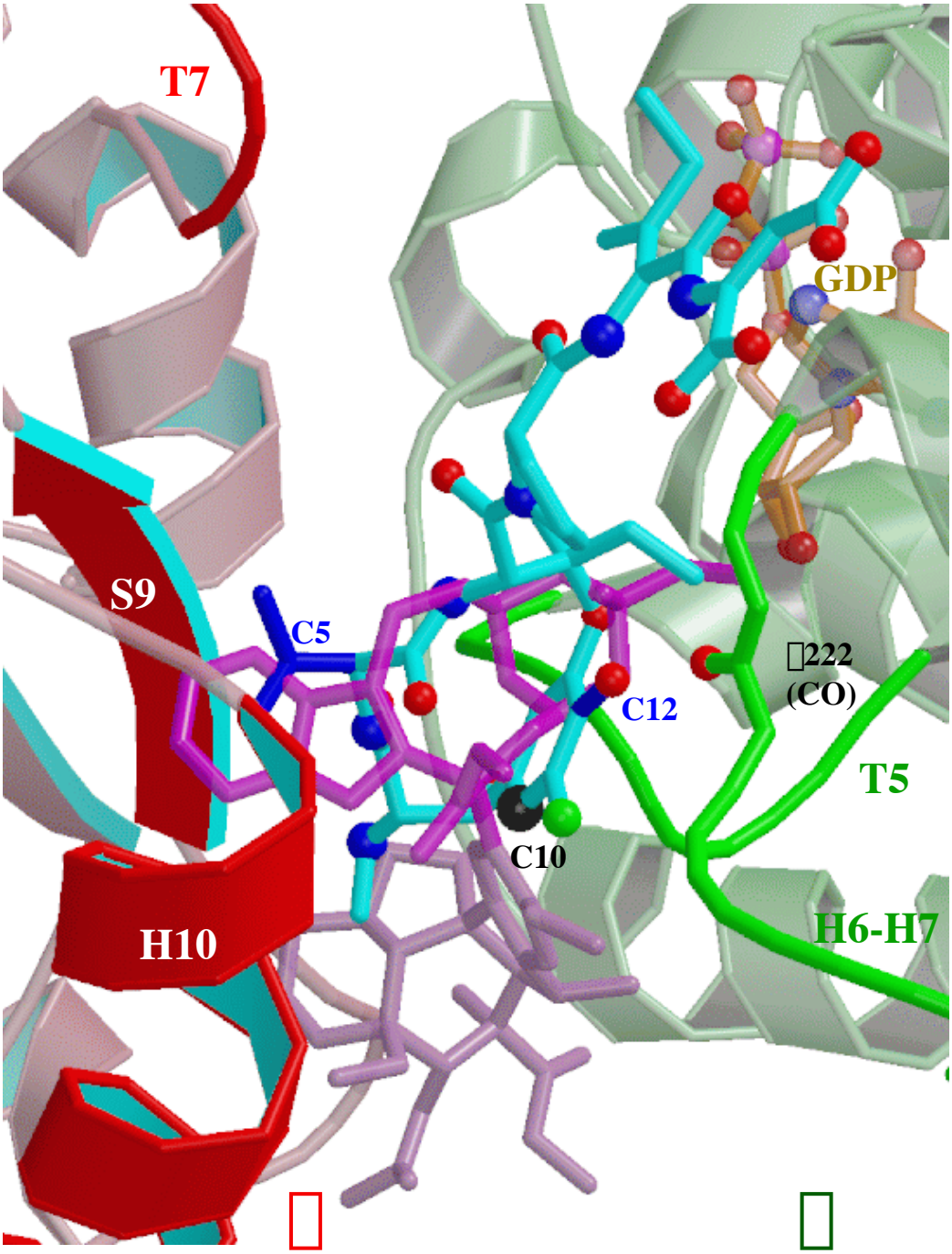

Supplementary Figure 2

A

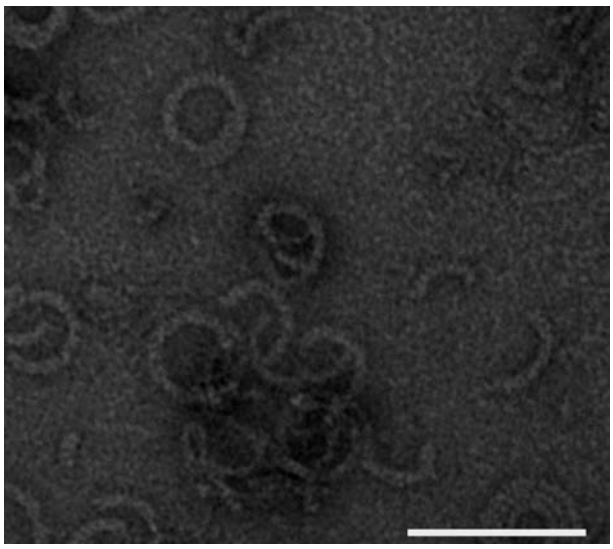

B

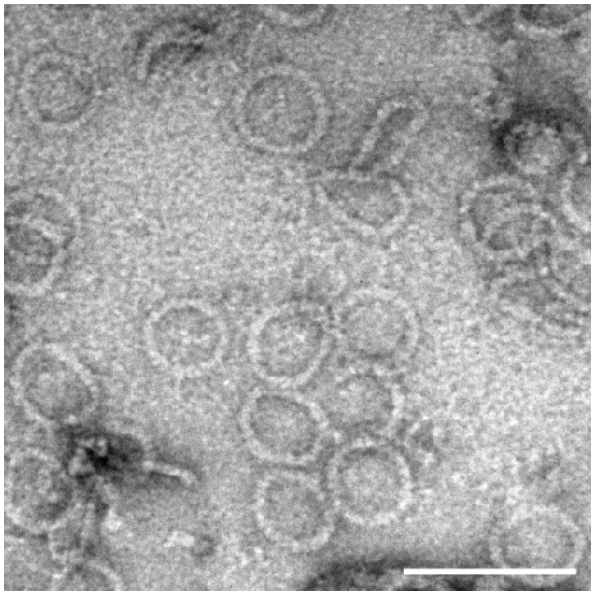

C

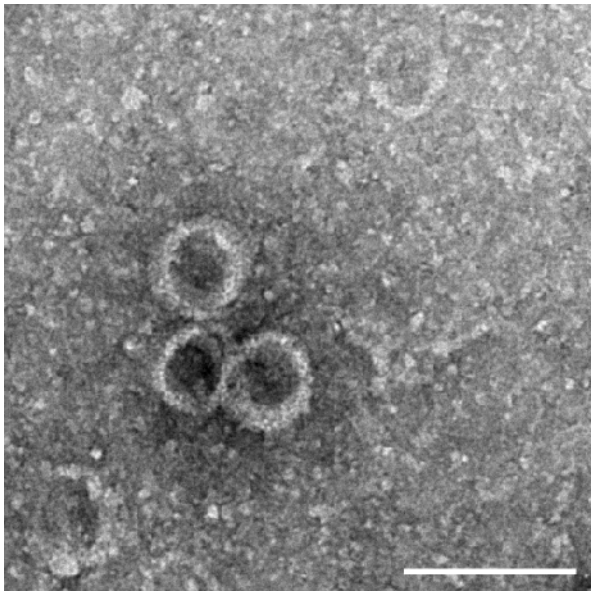

Supplementary Figure 3

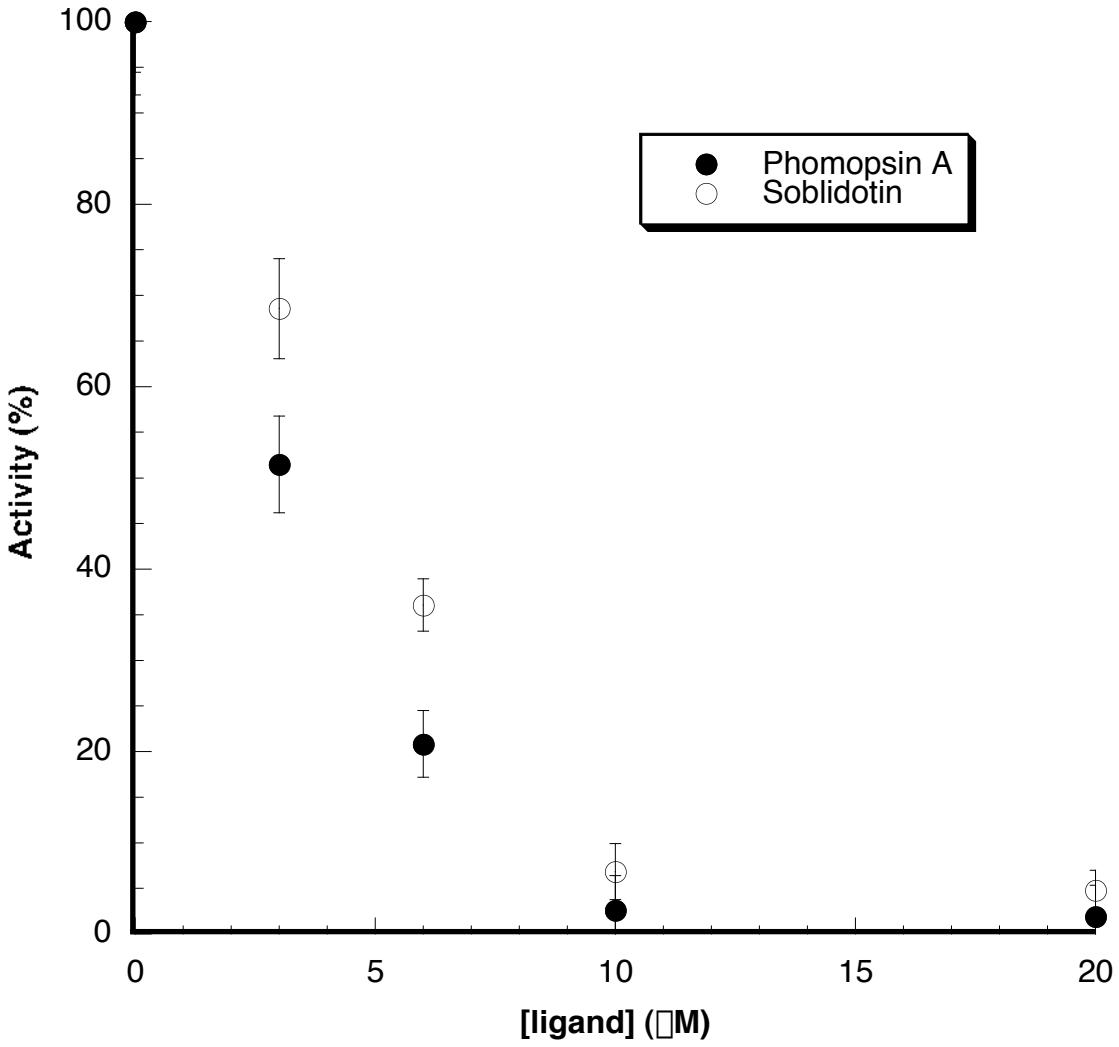

Supplementary Figure 4

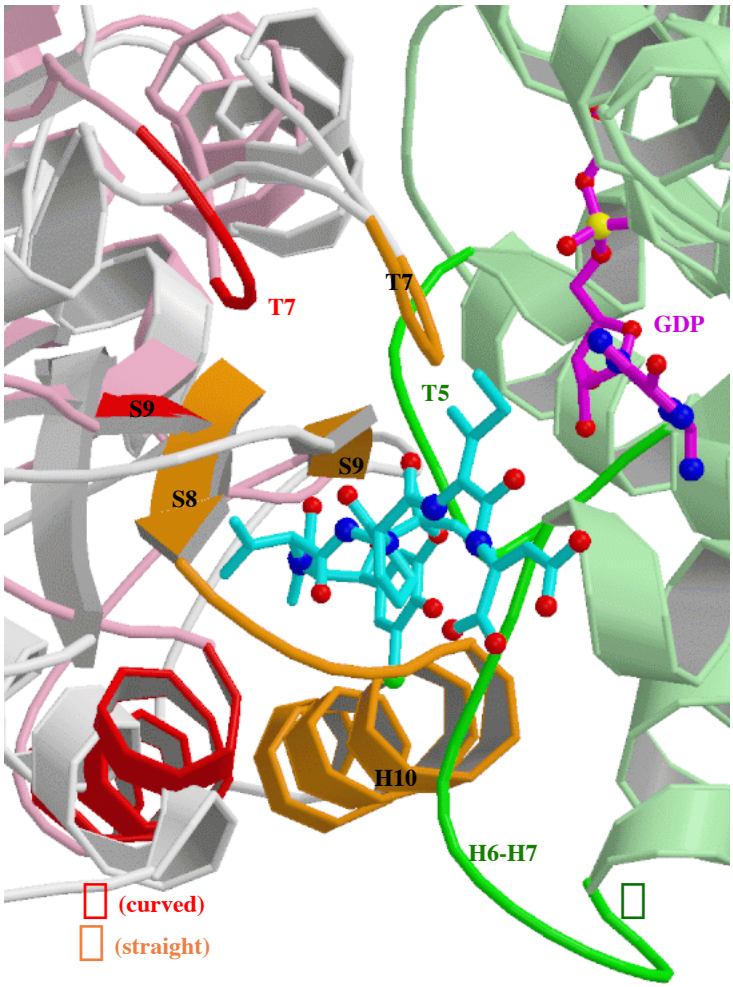

Supplementary Figure 5

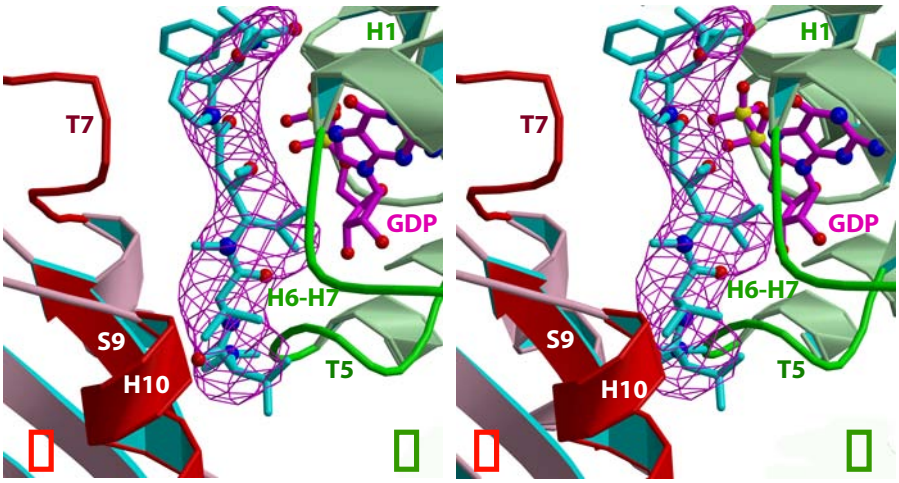

Supplementary Figure 6